Supplement of Solid Earth, 9, 1207–1224, 2018
https://doi.org/10.5194/se-9-1207-2018-supplement

Solid Earth
Open Access

Supplement of

The influence of upper-plate advance and erosion on overriding plate deformation in orogen syntaxes

Matthias Nettesheim et al.

Correspondence to: Todd A. Ehlers (todd.ehlers@uni-tuebingen.de)

	Upper Crust Wet Granite[a]	Lower Crust Dry Diabase[a]	Lithospheric Mantle Olivine aggregates[b]
Density ρ $[\mathrm{kg\,m^{-3}}]$	2750	2900	3300
Thermal Diffusivity $k/\rho c$ $[10^{-6}\,\mathrm{m^2\,s^{-1}}]$	1.0	1.0	1.0
Heat Production $[\mathrm{\mu W\,ka^{-1}\,m^{-3}}]$	1.8	0.6	0.0
Viscosity Prefactor B_0 $[\mathrm{Pa\,s^{1/n}}]$	$4.43{\cdot}10^7$	$1.24{\cdot}10^6$	$1.21{\cdot}10^7$
Activation Energy Q $[\mathrm{kJ\,mol^{-1}}]$	140.6	276.0	324.3
Stress Exponent n [1]	1.9	3.05	3.5
Cohesion C_0 [MPa]	10	10	2
Friction Angle ϕ [°]	$15 \rightarrow 5$	$15 \rightarrow 5$	10
Strain Weakening Interval [1]	$0.05 \rightarrow 0.55$	$0.05 \rightarrow 0.55$	-

a Carter and Tsenn (1987)

b Hirth and Kohlstedt (2003); Jadamec and Billen (2012)

Table S1. Overriding pate material parameters

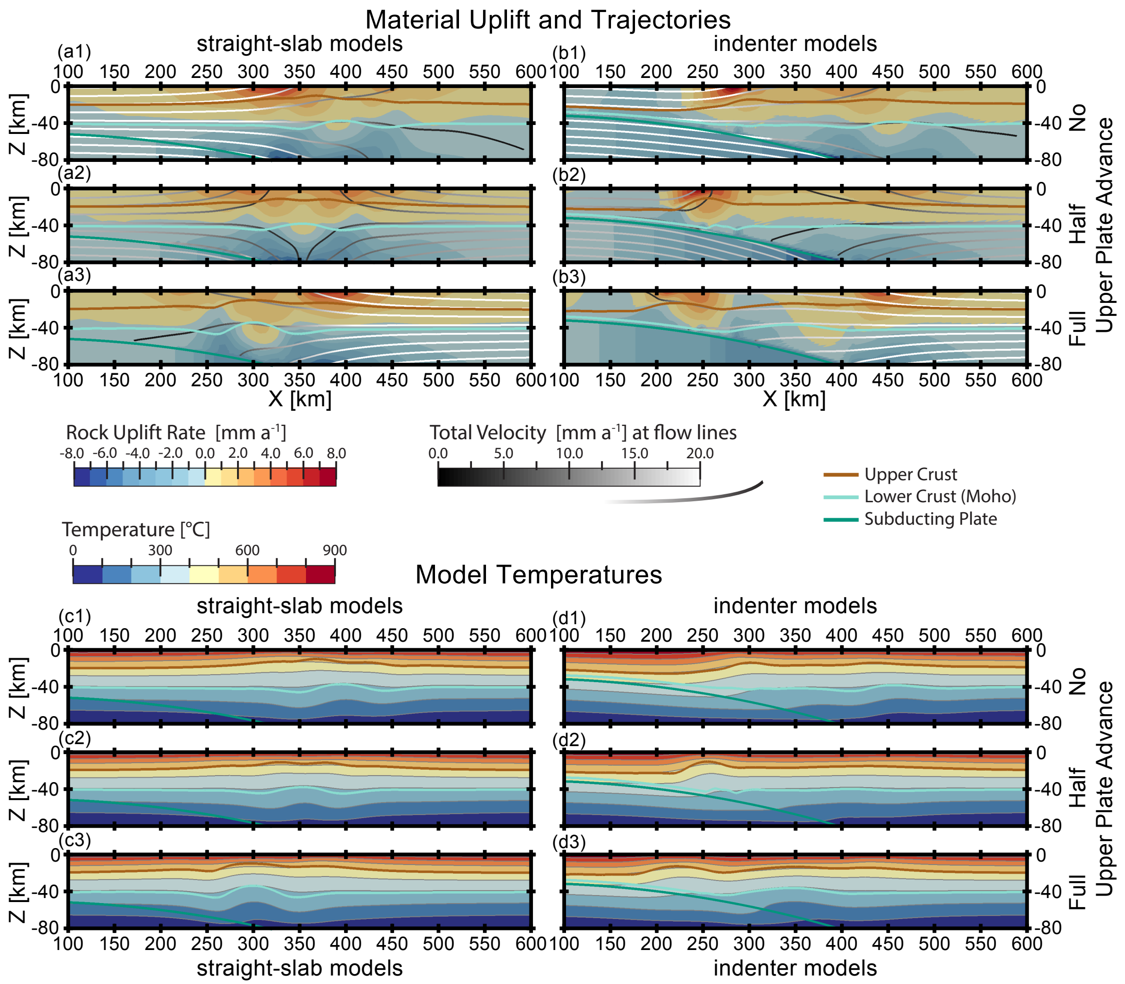

Figure S1. Comparison of velocities and temperatures between straight-slab (left column) and intenter-type (right column) flat erosion models (models 1–6). Colored lines denote material layer boundaries. Panels **(a1)**–**(b3)**: Background colors denote vertical velocity component, material flow lines are colored by total velocity. Panels **(c1)**–**(d3)**: Background color show temperatures. Colored lines denote material layer boundaries. Plots show the increased and focused uplift around $x = 250\,\mathrm{km}$ created by the indenter and the corresponding temperature anomalies, which mostly correspond to deformation.

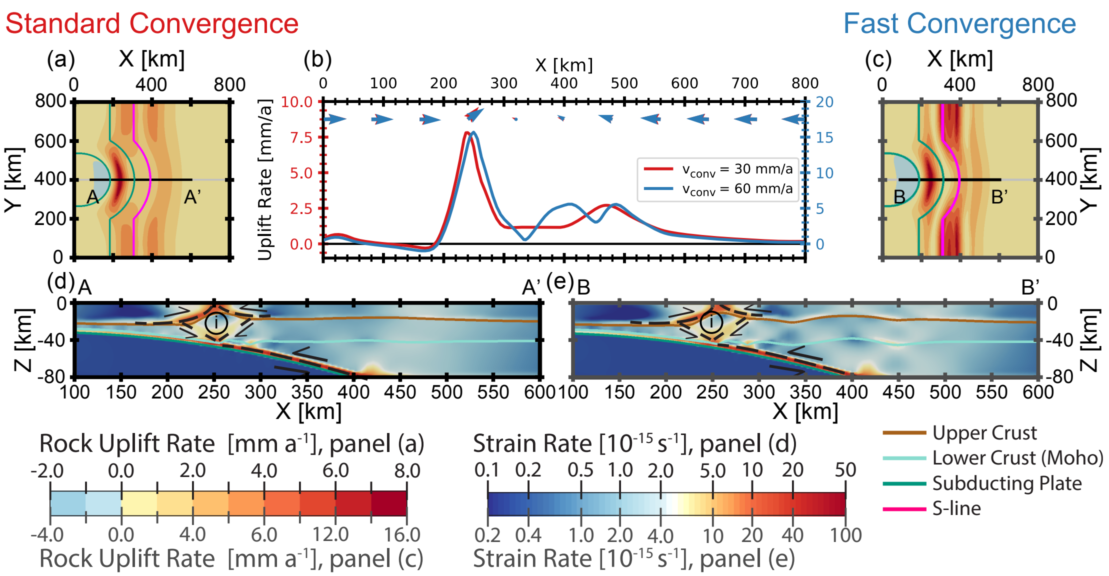

Figure S2. Comparison of standard and twice as fast convergence models (models 5 and 7) after 4 and 2 Myr modeling time, respectively (equal amount of material added to domain). Panels **(a)** and **(c)** show rock uplift rates, panels **(d)** and **(e)** strain rates at $y = 400$ km and panel **(b)** shows surface rock uplift rates along $y = 400$ km slice. Please note that all scales for fast convergence model are doubled (gray labels), but relative distribution of rock uplift and strain rates is almost the same.

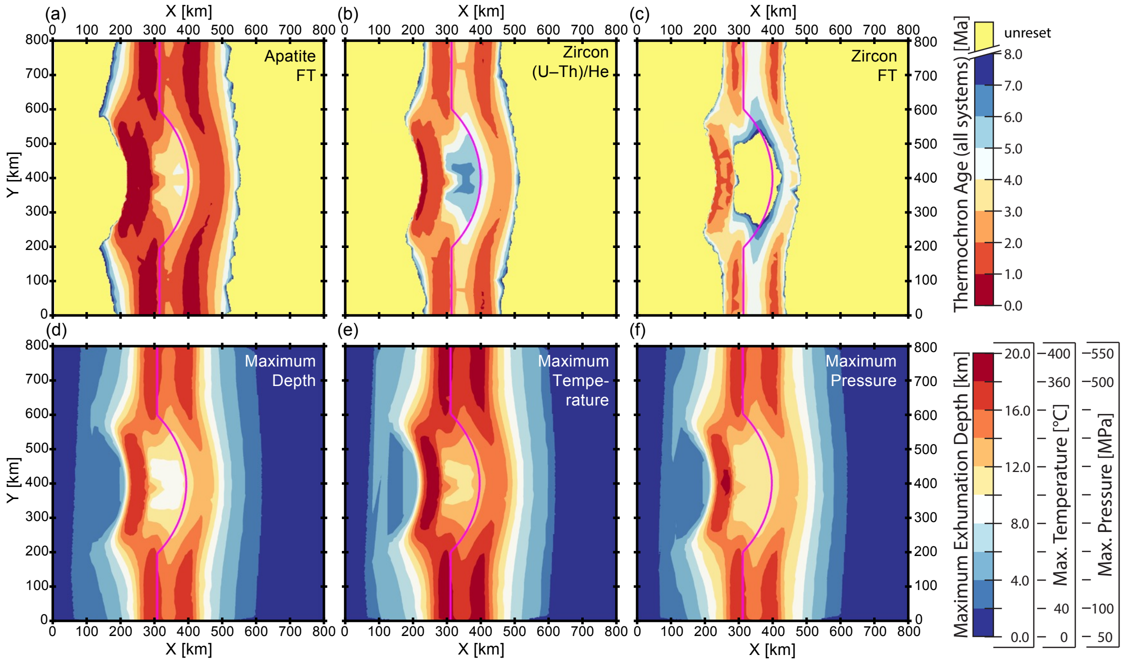

Figure S3. Thermochronometric cooling ages (Apatite fission track ($T_c \approx$120 °C), Zircon (U–Th)/He ($T_c \approx$180 °C), and Zircon fission track ($T_c \approx$240 °C)), as well as physical exhumation parameters (maximum depth, temperature, and pressure) of the half advance indenter model (model 5) after 8 Myr simulation time. All observables clearly follow the pattern set by rock uplift rates of two bands to the front and back, as well as a region of localized uplift above the indenter (see Figs. 4b3 and 5b). Thermochronometric age is increasingly older with a higher closing temperature of the respective system (from left to right). The cooling ages above the indenter are slightly but consistently younger than those related to the pro and retro shear zone at the model front and back ($y < 200$ km and $y > 600$ km, respectively).

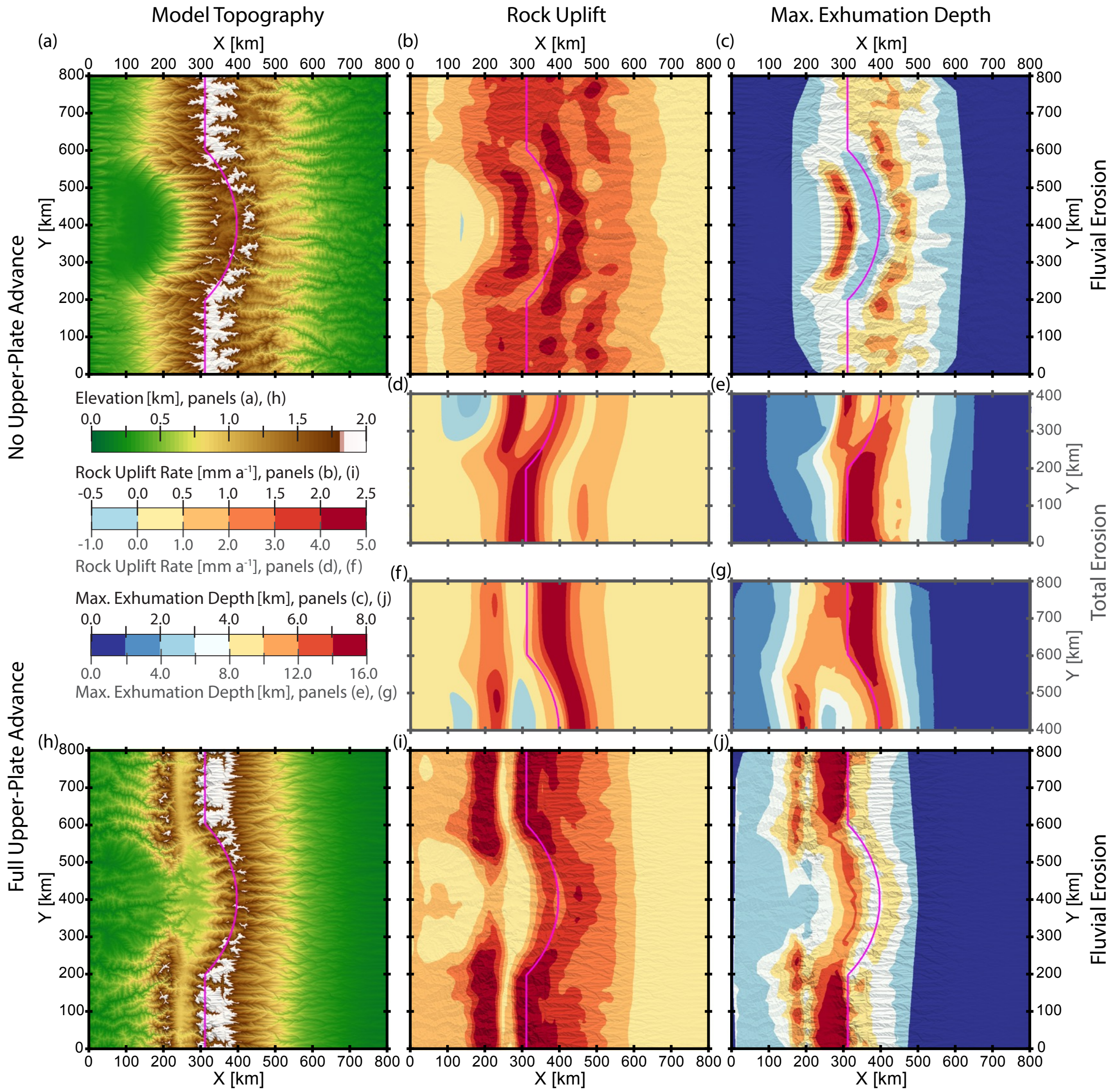

Figure S4. Comparison of rock uplift and exhumation depths with fluvial versus total erosion for no (model 10, upper half) and full (model 12, lower half) upper plate advance. **(a)** and **(h)** surface elevations, **(b)** and **(i)** rock uplift rates, and **(c)** and **(j)** exhumation depth after 6.0 Myr modeling time. Uplift is focused more toward the center for the no advance and more to the front and back for the full advance fluvial erosion model. **(d)**, **(e)**, **(f)**, and **(g)** show the respective flat erosion results (models 4 and 6) for rock uplift rates and exhumation depth for comparison. Note the range is increased by factor 2 for those four plots (gray labels).